Proceedings of the International Conference on Structural Health Monitoring of Intelligent Infrastructure
Porto, Portugal, 30 June - 2 July 2021
ISSN 2564-3738

Anomaly detection and localization on masonry arch bridges using frequency data

Paolo Borlenghi[1], Antonella Saisi[1], Carmelo Gentile[1]
[1] Department of Architecture, Built environment and Construction engineering (DABC), Politecnico di Milano, Piazza Leonardo da Vinci 32, 20133 Milan, Italy
email: paolo.borlenghi@polimi.it, antonella.saisi@polimi.it, carmelo.gentile@polimi.it

ABSTRACT: Despite the age of construction, masonry arch bridges and viaducts have still an essential role in the European infrastructural network, so that implementing techniques to control their health state is of primary interest. To this purpose, masonry viaducts - often characterised by high piers - can be continuously monitored with Operational Modal Analysis (OMA): this technique provides reliable information on the natural frequencies of the structure and the possible appearance of structural anomalies. Nevertheless, due to the complexity of masonry viaducts, to move from damage detection to localisation with a relatively simplified distribution of sensors, a calibrated numerical model is needed. The paper summarises the development of a Structural Health Monitoring (SHM) methodology for the model-based damage assessment in masonry arch bridges using frequency data. The proposed methodology involves the following steps: (i) preliminary analysis including architectural research and OMA; (ii) FE modelling and updating based on the identified modal parameters; (iii) creation of a Damage Location Reference Matrix (DLRM) from numerically simulated damage scenarios; (iv) detection of the onset of damage from the analysis of the continuously collected natural frequencies, and (v) localisation of the anomalies through the comparison between the experimentally identified variations of natural frequencies and the DLRM. The proposed SHM methodology is exemplified on the *Olla* bridge, Piedmont region, Italy. Pseudo-experimental monitoring data were generated and used to assess the reliability of the developed algorithm in identifying the damage location. The results show a promise toward the practical applications of the proposed strategy for the early identification of damage in masonry viaducts.

KEY WORDS: Damage localisation; Arch bridges; Model updating; Historical constructions; Structural Health Monitoring.

1 INTRODUCTION

Within the context of Structural Health Monitoring (SHM), the identification of damage at an early stage of deterioration is of utmost importance for masonry arch bridges. These structures were built several decades ago, and many of them are still in use today, representing essential infrastructures for the European road and railway networks [1].

Recent full-scale experiences on historical structures [2]-[3] provided evidence that the analysis of continuously identified natural frequencies can reveal the onset of damage under changing environment. Employing natural frequencies as a damage-sensitive feature is especially of interest for masonry viaducts: due to their complex structural arrangement, monitoring the mode shapes evolution accurately – as it is usually done in beam-like structures – might require a complex sensor layout. Conversely, measuring the bridge response in the middle of arches and piers at the deck level is suitable to identify a relatively large number of natural frequencies and perform damage detection.

Figure 1. The *Olla* bridge, view from the Stura river.

However, damage detection represents only the first level (Level 1) of damage assessment in the classification initially proposed by Rytter [4] and does not answer essential questions on damage localisation (Level 2) and the evaluation of its severity (Level 3). Therefore, to move from detection to localisation using a relatively simplified sensor layout, a calibrated numerical model is needed to investigate how damage in a specific location affects the mutual variation of natural frequencies.

The objective of the paper is to extend the capability of vibration-based monitoring systems for masonry bridges towards an effective damage localisation using frequency data. To this purpose, the information extracted from a dynamic monitoring system is integrated with the ones obtained from a baseline Finite Element (FE) model. The methodology – similarly to what has been proposed for the masonry towers [5] – involves the subsequent steps: (i) calibration of the numerical model of the structure in the undamaged state, (ii) creation of a reference location matrix from numerically simulated damage scenarios, (iii) assuming that the structure is permanently instrumented, after the cleansed natural frequencies have detected the onset of some anomaly, the anomaly position is defined through the comparison between the experimentally identified frequency

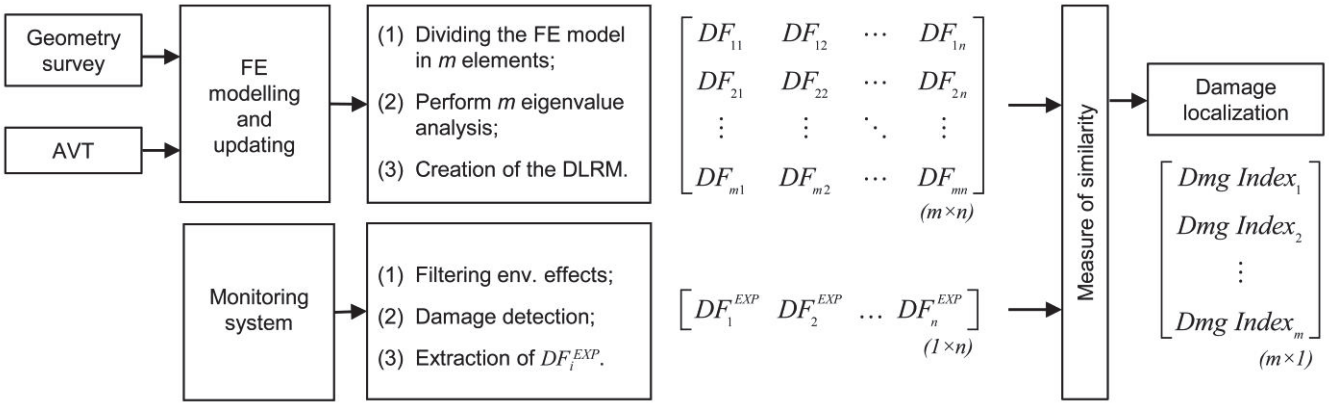

Figure 2. Proposed damage identification scheme.

variations and the above-defined location matrix, containing information on the numerically simulated damage scenarios.

Compared to previous studies using a sensitivity-based approach (see e.g. [6]-[7]), the present technique is not limited to academic examples or very simple structures and can be applied to three-dimensional structures such as masonry arch bridges.

The 19th-century *Olla* bridge (Figure 1) is used to exemplify the proposed approach. The bridge, 117 m long, comprises five arches, four piers and two abutments; the arches are built in solid brick masonry, whereas piers and abutments are made of a good-quality ashlar stone masonry. The bridge crosses the Stura river along the National Road S.S. 21, connecting the French border with the South-West part of Piedmont region, throughout the Stura di Demonte valley. The development and the calibration of a numerical model of the historical bridge, based on ambient vibration tests, is firstly reported: the investigated structure turns out to be of particular interest because the use of just 14 sensors allows the identification of a relatively large number of natural frequencies (so that the installation of a dynamic monitoring system on the bridge has been scheduled). Pseudo-experimental monitoring data are then generated from the updated model and employed to assess the reliability of the proposed algorithm in identifying the damage location.

2 DAMAGE IDENTIFICATION METHODOLOGY

The proposed SHM methodology (Figure 2) is conceived to use the observed changes in natural frequencies to localise the onset of damage in continuous monitoring systems.

Firstly, the numerical model of the investigated structure is developed and calibrated based on preliminary investigations, namely, geometric survey and ambient vibration testing.

The calibrated numerical model is then divided into m regions with homogenous material properties. The number and the distribution of the localisation regions depend on the geometry of the investigated structure and should be defined using engineering judgement. Differentiating arches and piers from the rest of the structure can be considered a general value choice for masonry bridges.

Subsequently, m eigenvalue analyses are performed reducing the elastic modulus of each region by a certain quantity (e.g., the 40%). The resulting changes in the n considered natural frequencies – measured with a discrepancy function, Eq. (1) – are collected in an $m\times n$ matrix called Damage Localisation Reference Matrix (DLRM).

Simultaneously, a monitoring system is installed on the investigated structure, and the natural frequencies are identified and tracked by applying state-of-art techniques. The fluctuations caused by the environmental and operational effects are removed using regression analysis (e.g., PCA-based regression [8]). For this purpose, the structure is analysed during a reference period – usually called training period – to study the effects of temperature, vehicular traffic, and other external factors. Once the training period is completed, the occurrence of structural anomalies is investigated through the residual errors between predicted and identified frequency data (see e.g. [9]).

Control charts are then used to detect the anomalous variations in the data. Control charts are graphical representations of the evolution over time of a particular process with designed control limits: an observation is considered abnormal when the control limit is exceeded. In SHM, the control limits are evaluated during the training period when the structure is assumed to be undamaged. The successful use of control charts for the damage detection of real-monitored structures has been reported by [2] and [3]. In this paper, the Hotelling multivariate control chart based on the T^2 statistic [10] is adopted.

Once an anomaly has been detected, the corresponding frequency shifts must be obtained. Since the residuals are affected by a certain variability, a mean value of H hours (e.g., 48 hours) is defined for both the undamaged and the damaged state. Notably, the mean of the residuals in the undamaged state should be very close to zero, while the mean of the residuals in the damage state should correspond with the correct frequency shift. Consequently, a vector with n experimental frequency shifts is defined.

The effects of the damages on the natural frequencies – both numerically simulated and experimentally measured – are described through a discrepancy function, defined as:

$$DF_i = \frac{f_i^u - f_i^d}{f_i^u} \cdot 100 \qquad (1)$$

where the i-th natural frequency before and after the damage occurred is represented by f_i^u and f_i^d, respectively.

By computing the similarity between the frequency shifts in the DLRM and the ones given by the cleaned observations, it

is possible to locate where the anomaly appeared. Notably, the Cosine Similarity is adopted to measure the similarity between the vector of the identified experimental frequency shifts ($\boldsymbol{DF}_{EXP}$) and the m vectors of the simulated damage scenarios ($\boldsymbol{DF}_j$):

$$\cos\theta_j = \frac{\mathbf{DF}_j \cdot \mathbf{DF}_{EXP}}{\left\|\mathbf{DF}_j\right\| \cdot \left\|\mathbf{DF}_{EXP}\right\|} \tag{2}$$

where θ_j is the j-th angle between the two vectors. It is worth noticing that values of cos θ_j close to 1 suggest a good correlation with the identified frequency shifts while values lower than 0.9 suggest a poor correlation.

In the present paper, the adopted Damage Index (DI) is expressed as follow:

$$DI_j = (1-\cos\theta_j)^{-0.5} \tag{3}$$

The m DI are then plotted together to better understand the results and the localisation is performed considering the region associated with the higher DI.

3 DESCRIPTION OF THE OLLA BRIDGE

The *Olla* bridge (*Ponte dell'Olla* in Italian, Figure 1) is a multi-span masonry arch bridge built in the second half of the 19th century over the Stura river. It carries the State Route no. 21 (SS21, i.e., the roadway connecting the city of Cuneo with the French border) between the municipalities of Gaiola and Borgo San Dalmazzo in the northwest part of Piedmont, Italy. Due to its localisation, the bridge has a strategic role for the economy of the area since it is the only entry to the Stura di Demonte Valley for trucks and commercial vehicles.

The structure is approximately 117 m long and has a maximum height over the river of about 42 m. It is composed of five masonry arches, symmetrically distributed, with spans of 10, 20, and 25 m, respectively. Piers and abutments are in a good quality ashlar stone masonry while arches and spandrel walls are in brick masonry. The documentary research started in the archive of the Local Authority responsible for the design (*Genio Civile*), but the original drawings were not found. Therefore, various construction details on the internal morphology of the structure were initially assumed according to the historical construction handbooks of Curioni [11] and then eventually modified in establishing the FE model.

In order to obtain a complete representation of the existing structure, a topographic survey was performed in September 2018 [12] using a total station (Leica TCRA 1203) and a laser scanner (Leica C10). Hence, the survey relied on different techniques, integrating local and global measurements, ensuring a 360° coverage of the bridge complexity. The 3D model resulting from point clouds was used to extract 2D drawings from which the FE model was developed.

Moreover, the historical research revealed that during the Second World War, the *Olla* bridge was heavily damaged, leading to the collapse of the central arch. According to Taricco [13], the structure was detonated by the partisans on July 13th, 1944 to isolate the valley from the German army. The bridge was repaired starting from September 1945 [13], and the central arch reconstructed; however, no specific records were found on the execution of the intervention.

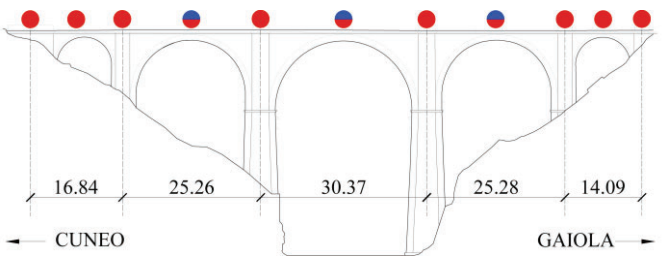

Figure 3. Sensors layout during the AVT (dimensions in m): the red and blue dots refer to transverse and vertical sensors, respectively.

4 PRELIMINARY EXPERIMENTAL SURVEY

The experimental survey conducted on the *Olla* bridge included Ambient Vibration Tests (AVTs) and Minor Destructive Tests (MDTs).

The AVT was performed on July 31st, 2018, with one lane open to traffic; the acceleration responses of the bridge were measured in 11 selected points belonging to the downstream side of the deck. As represented in Figure 3, the sensor layout was designed to guarantee a complete representation of the lateral mode shapes (11 transversal sensors), and a partial reconstruction of vertical and longitudinal ones, deploying 3 vertical sensors placed in the centre of the major arches, where the maximum modal displacements were expected.

During the test, 14 piezoelectric accelerometers with a 10

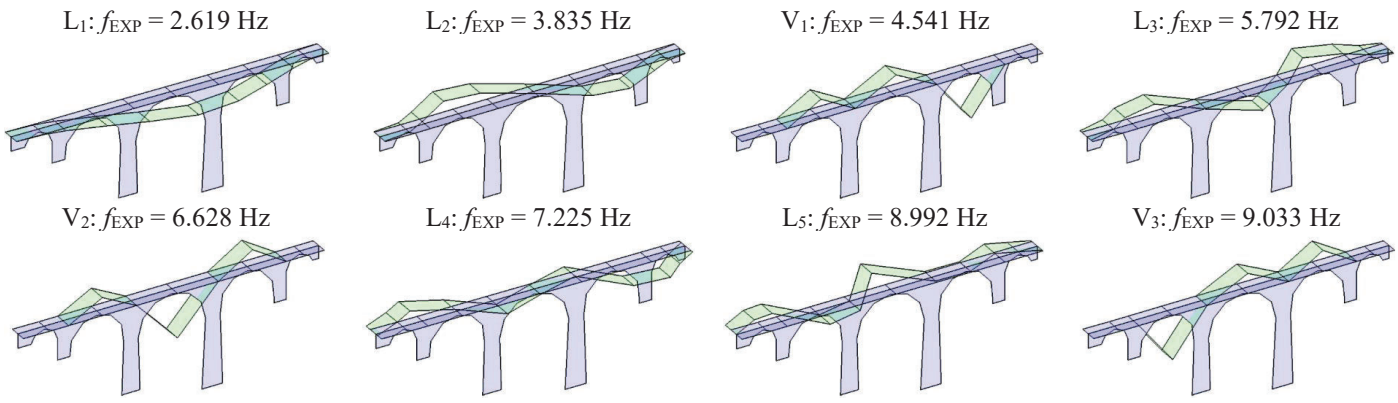

Figure 4. Identified vibration modes (L = dominant lateral, V = dominant vertical).

V/g sensitivity were used. The sampling frequency adopted was equal to 200 Hz, which is more than enough for the considered structure whose dominant frequencies are below 10 Hz. Therefore, low pass filtering and decimation were applied to down-sample the data to 40 Hz, obtaining a Nyquist frequency of 20 Hz.

The modal identification was performed by applying a fully automated algorithm, based on the Covariance-based Stochastic Subspace Identification (SSI-Cov) method [14] and developed within a previous research [15]. The natural frequency estimates have also been verified through the well-known technique of Frequency Domain Decomposition [16]. Overall, 5 lateral and 3 vertical vibration modes are identified in the frequency range of 0-10 Hz (Figure 4).

Subsequently, the MDTs – consisting of limited coring tests – were performed to obtain information on arches, spandrels and fill. Due to the limited extension of the core drill machine, no information on the backing was obtained. The coring tests were executed in Autumn 2018. Six coring samples were taken from the following elements: 2 on the arches, 2 on the spandrels and 2 on the deck. The tests revealed that the arches are constituted only by brick masonry while the spandrels are a mixed of stone and brick masonry. The fill – as expected – is constituted by compacted soil and pebbles. The thickness of the asphalt, over the fill, is equal to 20 cm.

5 FE MODELLING AND UPDATING

The 3D model of the *Olla* bridge was developed with the FE code ABAQUS using the ten-node tetrahedral elements (C3D10). A relatively large number of elements were employed to obtain a regular distribution of masses, a good description of geometrical details, and to avoid frequency sensitivity to mesh size. Overall, the numerical model consists of 45604 tetrahedral elements with 211818 degrees of freedom and an average mesh size of 1.15m (Figure 6).

Once the geometry of the numerical model is established, the selection of the structural parameters to be updated is the next key issue. To prevent the ill-conditioning of the inverse problem and to improve the robustness of the updated parameter estimates, the following aspects were considered: (i) the number of updating variables was kept smaller than the experimental parameters used as targets; (ii) only the uncertain structural parameters were updated; (iii) the sensitivity of natural frequencies to the different parameters was checked and low-sensitivity structural parameters were not updated.

Overall, 8 regions with constant material properties were identified based on visual inspections and coring tests (see Figure 6): 1. piers and abutments; 2. the central arch (reconstructed in 1945); 3. lateral arches; 4. spandrels; 5. the base of central piers; 6. the backing over the abutments and the lateral piers; 7. the backing over the central piers (partially reconstructed in 1945); (8) the fill.

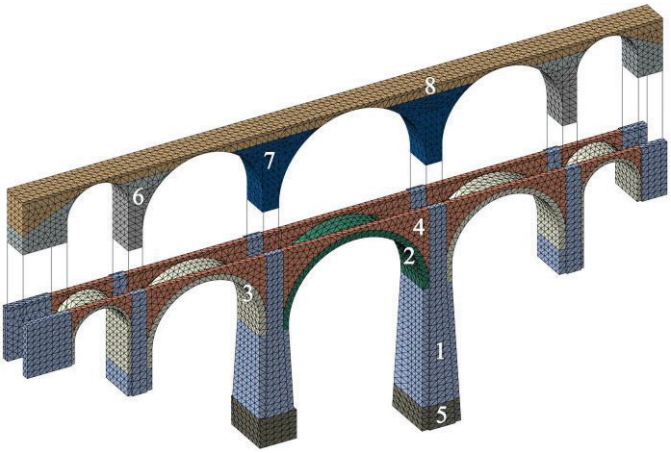

Figure 6. FE model with the indication of different materials: 1. Piers; 2. Central arch; 3. Lateral arches; 4. Spandrels; 5. Pier foundations; 6. Backing; 7. Central backing; 8. Fill.

In addition, the following assumptions were adopted: (a) the effect of soil-structure interaction was neglected, (b) all the materials were considered isotropic with constant mass density and Poisson's ratio (Table 1), (c) the spandrels were assumed 1.0 m thick, and (d) the Young's modulus of fill material was not adjusted due to its low sensitivity. Given the clear presence of superficial rocks at the river level, the base nodes of piers and abutments were assumed pinned. Similarly, the longitudinal translation of the abutments was restrained.

A one-to-one correspondence between the experimental and numerical vibration modes was obtained with the initial FE model, providing a sufficient verification to the main modelling assumptions. Nevertheless, the discrepancy – in terms of natural frequencies – was still quite high, with a maximum value larger than 7%.

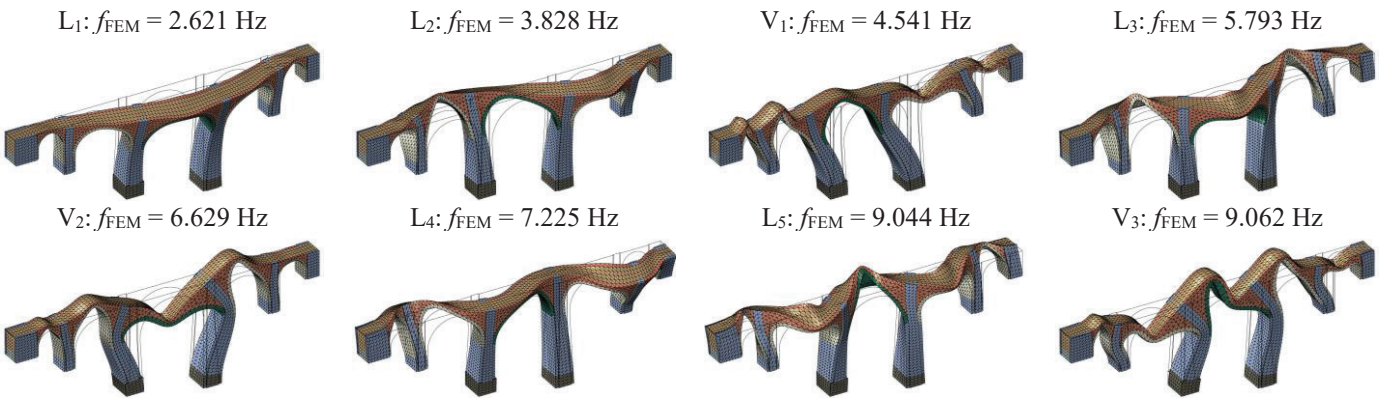

Figure 5. Lateral (L) and vertical (V) vibration modes of the optimal (updated) FE model.

Table 1. Summary of the assumed (*) and identified structural parameters.

No.	Structural elements	ν *	γ (kN/m^3) *	E (GPa)
1	Piers / abutments	0.15	20	16.10
2	Central arch	0.15	17	7.73
3	Lateral arches	0.15	17	3.23
4	Spandrels	0.15	19	16.85
5	Pier foundations	0.15	21	27.49
6	Lateral backing	0.15	18	1.38
7	Central backing	0.15	18	4.56
8	Fill *	0.30	16	0.30

Table 2. Comparison between experimental (SSI-Cov) and numerical frequencies (Updated model).

Mode		Exp.	Optimal model	
No.	Type	f_{AVT} (Hz)	f_{FEM} (Hz)	DF (%)
1	L_1	2.619	2.621	–0.07
2	L_2	3.835	3.828	0.18
3	V_1	4.541	4.541	–0.01
4	L_3	5.792	5.793	–0.02
5	V_2	6.628	6.629	–0.02
6	L_4	7.225	7.225	–0.01
7	L_5	8.992	9.044	–0.57
8	V_3	9.033	9.062	–0.32
DF_{ave} (%)		–	–	0.15
DF_{max} (%)		–	–	0.57

To enhance the correlation with the experimental response, a model updating procedure was implemented in the MATLAB environment based on the Douglas-Reid method [17] with the Particle Swarm Optimisation (PSO) algorithm [18]. The updating parameters were iteratively corrected in a constrained range until a minimum solution for the following objective function was found:

$$J(\mathbf{x}) = \frac{100}{n}\sum_{i=1}^{n}\left|\frac{f_{AVT,i} - f_i^*(\mathbf{x})}{f_{AVT,i}}\right| \quad (4)$$

where $f_{AVT,i}$ are the i-th experimentally identified natural frequency and $f_i^*(\mathbf{x})$ are the i-th polynomial approximations [17] of the numerical natural frequencies, expressed as functions of the $\mathbf{x}$ updating parameters.

Table 1 lists the optimal estimates of the uncertain parameters of the model while Table 2 illustrates the excellent correlation of the updated model with the experimental results (DF_{ave} = 0.15%). The differences between the Young's modulus of the central and lateral arches, as well as the one of the backing, are motivated by the different years of construction: as shown by the historical analysis, the central arch was rebuilt in 1945. As demonstrated by the coring tests, the spandrels are made of bricks externally and stone internally, justifying the high values of Young's modulus. Finally, the base of the central piers is built in a better quality stone masonry in respect to the rest of the piers and, moreover, the optimal elastic modulus conceivably accounts for the stiffening effect provided by the compacted soils surrounding the piers.

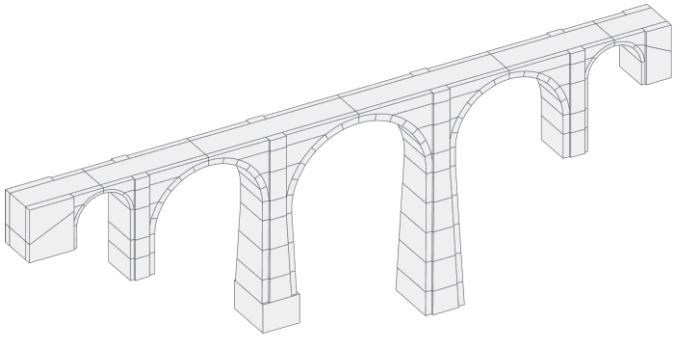

Figure 7. Division of the optimal FE model in 125 regions.

6 DEFINITION OF THE DAMAGE LOCALISATION REFERENCE MATRIX (DLRM)

The damage location matrix was created employing the previously optimised numerical model.

As shown in Figure 7, the model was divided into a relatively large number of regions to capture the possible effect of local damages. In detail, the main elements of the bridge are considered separately, namely arches, piers, abutments, backing, fill and spandrels. Moreover, each structural element was divided into smaller regions, as follow: the two lateral arches in 7 regions each one; the three central arches in 14 regions each one; the abutments in 2 regions each one; the two lateral piers in 1 region each one; the central piers in 4 and 5 regions; the backing in 14 regions; the fill in 6 regions; the spandrel walls in 34 regions.

Overall, 125 regions were identified, and the frequency sensitivity was computed according to Eq. (1). The elastic modulus of each region was decreased by 40%, and 125 eigenvalue analyses were performed, collecting the resulting variations of natural frequencies in the reference matrix.

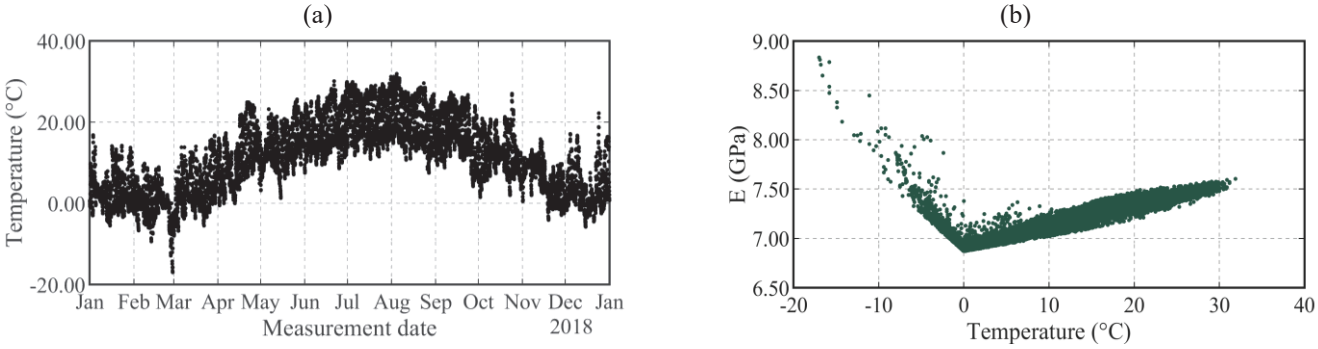

Figure 8. (a) Temperatures from Demonte weather station; (b) Temperature-Young's modulus correlation of the central arch.

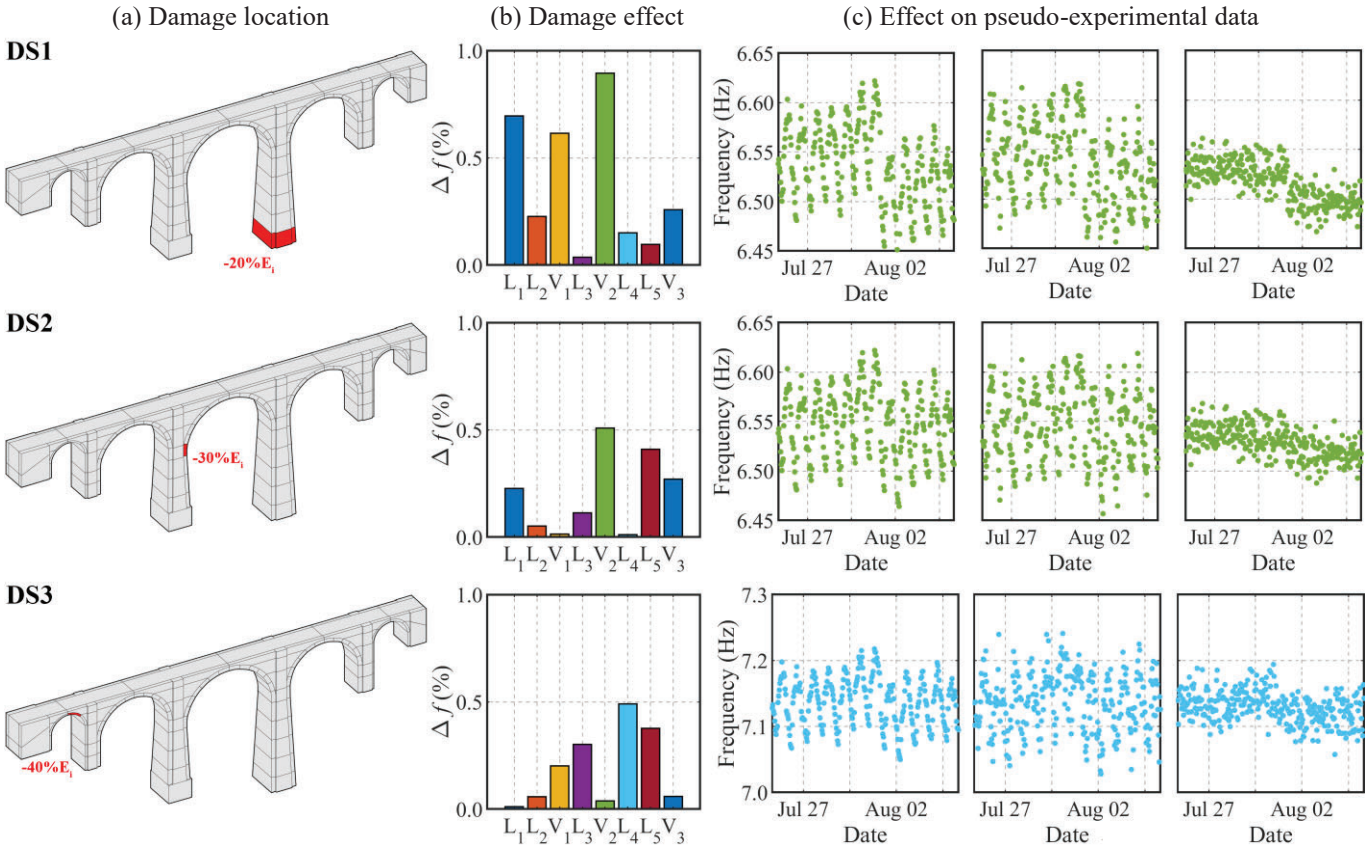

Figure 9. Simulated damage scenarios (DS): actual location, percentage variation of natural frequencies and 12-days zooms of the natural frequencies most affected by the damage.

7 PSEUDO-EXPERIMENTAL MONITORING DATA

To test the proposed model-based methodology for the damage identification, different damage scenarios (DS) were simulated on the pseudo-experimental monitoring data of the *Olla* bridge. The frequency data were generated based on the assumption that the structural response is affected only by the temperature changes. Therefore, the optimised FE model and the collected external temperatures were used to generate the variations of natural frequencies over one year. Subsequently, the environmental effects were removed using PCA-based regression, and the damage identification was performed with the proposed DLRM approach. The damage scenarios are assumed as permanent shifts on the natural frequencies, affecting only the stiffness of small portions of the masonry walls.

Firstly, the temperature data (Figure 8a) between January 2018 and December 2018 were retrieved from the Demonte weather station, which is about 9 km far from the investigated structure. The data were provided by the Regional Agency for Environmental Protection (ARPA) of Piedmont. As shown in Figure 8a, the temperatures of the winter months are often below zero degrees: it is worth noticing that in 2018, a sudden drop at the end of February up to −17°C was recorded. Consequently, considering the stiffening effect given by the low temperatures was fundamental to obtain reliable predictions of pseudo-experimental natural frequencies. To this purpose, the empirical relation between the elastic modulus and the air temperature was calibrated based on the work [19] on the Sciri tower of Perugia. In the latter research, an evident rise in natural frequencies was identified with temperatures below zero degrees.

As shown in Eq. (5), above zero degrees, the elastic modulus increases with the increase of temperatures and, below zero degrees, the elastic modulus increases with the decrease of temperatures. In more details, it has been assumed that the *i*-th Young's modulus $E_{i,k}$ at time k depends on the temperature at the same instant k and the temperature of the previous 6 and 12 hours:

$$g(T_k) = \begin{cases} E_i^{AVT} \cdot \left(-0.0167 \cdot T_k - 0.0033 \cdot T^{AVT}\right) & \text{when } T_k < 0 \\ 0.0033 \cdot E_i^{AVT} \cdot (T_k - T^{AVT}) & \text{when } T_k \geq 0 \end{cases} \quad (5)$$

$$E_{i,k}(T_k) = 0.6 \cdot g(T_k) + 0.3 \cdot g(T_{k-6h}) + 0.1 \cdot g(T_{k-12h}) + E_i^{AVT} \quad (6)$$

where E_i^{AVT} is the *i*-th Young's modulus identified with the model updating procedure from the AVT data and T^{AVT} is the average temperature during the AVT.

Figure 8b illustrates the variations of Young's modulus of the central arch obtained from the empirical relationships Eqs. (5)-(6). The obtained variations of mechanical parameters were subsequently used to generate the time series of natural frequencies using the metamodel created for the model updating. Furthermore, to simulate the presence of noise on the generated data, a normal distribution with a pre-defined standard deviation was assumed for each frequency.

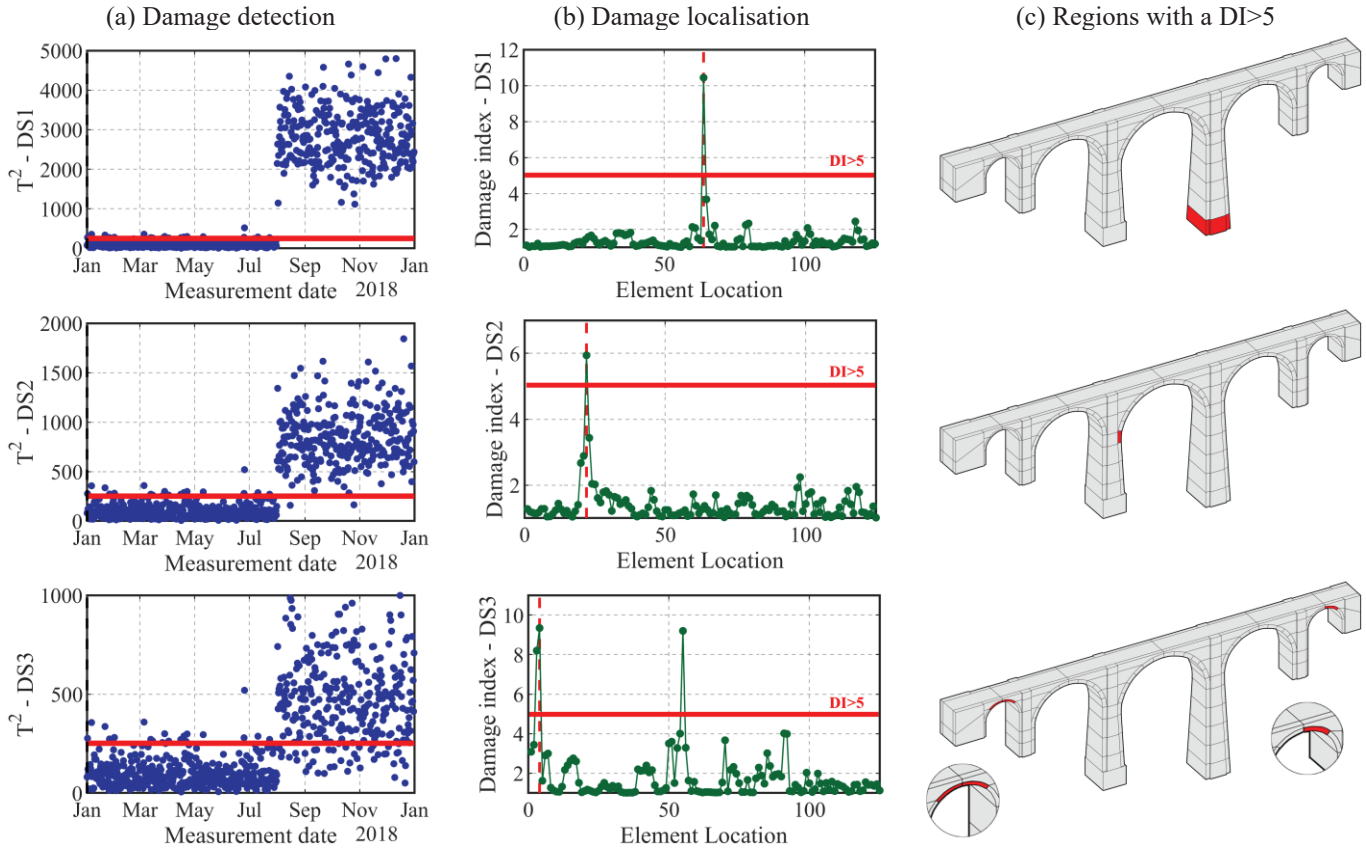

Figure 10. Damage detection and localisation for the three simulated damage scenarios.

Since the proposed damage identification strategy employs cleansed frequency data, the fluctuations caused by environmental effects were removed with a PCA-based regression using a training period of 6 months. The regression model is used to predict the modal frequencies after the training period, possibly revealing the presence of structural anomalies.

Subsequently, three damage scenarios (DS) were simulated (Figure 9a). The FE model was used to define the expected frequency decay (Figure 9b) while the DS were simulated on the pseudo-experimental data as permanent shifts in the natural frequencies (Figure 9c). In particular, the frequency shifts were obtained decreasing the elastic modulus of selected regions belonging to different parts of the structure: the first arch (DS1), the central arch (DS2) and the third pier (DS3). In more details:

- DS1 corresponds to 20% decrease in the Young's modulus of the basement of the third pier – the highest one – generating a maximum frequency shift of about 0.9% in the 5th mode (V_2);
- DS2 corresponds to 30% decrease in the Young's modulus of the skewback of the central arch, involving a maximum frequency reduction of about 0.5% in the 5th mode (V_2);
- DS3 corresponds to 40% decrease in the Young's modulus of a masonry portion belonging to the upper part of the first arch and induces a maximum frequency decrease of about 0.5% in the 6th mode (L_4).

The damage scenarios were simulated during the summer season (1st of August) when the daily frequency variations are higher. Subsequently, the random noise was added on the generated data, hiding the sharp changes of natural frequencies in the daily variations caused by environmental effects (Figure 9c); it is indeed impossible to recognize the frequency shifts inspecting the diagram.

8 DAMAGE DETECTION AND LOCALISATION

The residual errors obtained from the PCA-based regression were used to define a multivariate control chart based on the Hotelling's T^2-statistic [10]. The data were divided into subgroups of 12 hours, and a process mean was defined using a period of 6 months. The structural anomalies are detected each time an observation lays outside the control limit. As shown in Figure 10a, the three damage scenarios are clearly detected, and more specifically: (i) during the training period a limited number of observations exceed the control limit; (ii) at the time the damage is introduced, the control limit is suddenly exceeded by the T^2-statistic, exhibiting a more significant dispersion.

Once the presence of a structural anomaly is detected, the localisation is performed with the DLRM approach.

The pseudo-experimental frequency shifts were extracted from the cleansed observations as herein described.

- The values of the natural frequencies in the undamaged (f_u) state were defined as the mean of the training period – 6 month – while;
- The frequencies in the damage state (f_d) were defined as the mean of the 48 hours after the detection from the control chart.

The extracted frequency shifts – expressed in terms of percentage error, see Eq. (1) – were then compared with the

numerically computed frequency shifts –obtained from the 125 regions – using a measure of similarity (Eq. (2)). The Damage Index (DI) for each region was then computed using Eq. (3): the regions with a DI higher than 5 are most likely the regions in which the damage occurred.

As reported in Figure 10b and Figure 10c, the damage is correctly localised in the three cases. In Figure 10b the red dashed lines represent the correct damage locations, the green dots are the DI of each region, and the red continuous horizontal line identifies the DI higher than 5. In addition, Figure 10c highlights the regions with a DI higher than 5, showing the excellent localisation for DS1 and DS2 and a less effective localisation for DS3. As a consequence, the following comments can be drawn:

- The DS1 and DS2 are univocally localised in their exact location (Figure 10c);
- The DS3 is localised in both lateral arches (Figure 10c): the structure is quasi-symmetric longitudinally; consequently, it is not easy to distinguish between the contribution of the two lateral arches.

9 CONCLUSIONS

The paper focuses on the application of the proposed damage identification methodology for masonry viaducts – named DLRM – on the *Olla* bridge of Gaiola, Italy.

Firstly, the investigations included documentary research, geometric survey, and minor destructive and ambient vibration testing. Based on the information collected on-site, a three-dimensional FE model of the structure was developed, and the uncertain structural parameter optimised based on the identified modal parameters.

Subsequently, the application of the proposed damage identification procedure involved three main steps: (i) the creation of the DLRM using the optimised FE model divided into 125 regions; (ii) the simulation of three damage scenarios on the pseudo-experimental monitoring data of the *Olla* bridge; (iii) the data-driven damage detection using the residuals of the PCA-based regression and the subsequent localisation of the detected anomaly using a measure of similarity between the detected frequency shifts and the 125 numerically simulated frequency decays.

In summary, the following conclusions can be drawn:

- The documentary research on the *Olla* bridge revealed the collapsed central arch in 1944;
- During the AVT, performed with one line open to traffic, 5 lateral and 3 vertical vibration modes were identified in the frequency range of 0-10 Hz;
- Notwithstanding the initial model represented accurately the geometry retrieved from the geomatic survey, a relatively defective correlation with the actual structural response was obtained (DF_{ave} = 2.46%, DF_{max} = 7.35%);
- On the contrary, applying the model updating procedure and considering the effects of the reconstruction of 1945, an excellent correlation with the experimental results was obtained (DF_{ave} = 0.15%, DF_{max} = 0.57%), highlighting the importance of backing and spandrels in the dynamic response of masonry bridges;
- Three damage scenarios were simulated on the pseudo-experimental monitoring data. In all the considered cases, the damage was correctly identified and localised by using only the natural frequency changes.

ACKNOWLEDGMENTS

The support of ANAS (Struttura Territoriale Piemonte e Valle d'Aosta) is gratefully acknowledged. Sincere thanks are due to M. Cucchi and M. Iscandri (LPMSC, Politecnico di Milano) who assisted the authors in conducting the field tests.

REFERENCES

[1] A. Brencich, Masonry Bridges and Viaducts: Testing, Mechanics, Retrofitting Towards an Extended Life, *Structural Integrity* 11, 3-30, 2020.

[2] C. Gentile, M. Guidobaldi, A. Saisi, One-year dynamic monitoring of a historic tower: damage detection under changing environment, *Meccanica* 51(11), 2873-2889, 2016.

[3] F. Ubertini, N. Cavalagli, A. Kita, G. Comanducci, Assessment of a monumental masonry bell-tower after 2016 central Italy seismic sequence by long-term SHM, *Bull. Earthquake Eng.* 16(2), 775-801, 2018.

[4] A. Rytter, Vibration Based Inspection of Civil Engineering Structures, PhD thesis, Aalborg University, Denmark, 1993.

[5] P. Borlenghi, C. Gentile, A. Saisi, Detecting and localizing anomalies on masonry towers from low-cost vibration monitoring, *Smart Struct. Syst.*, in press.

[6] J.T. Kim, N. Stubbs, Crack detection in beam-type structures using frequency data, *J. Sound Vib.* 259(1), 145-160, 2003.

[7] A. Messina, E.J. Williams, T. Contursi, Structural damage detection by a sensitivity and statistical-based method, *J. Sound Vib.* 216(5), 791-808, 1998.

[8] I.T. Jolliffe, *Principal Component Analysis*, Springer, New York, NY, USA, 2002.

[9] F. Magalhães, A. Cunha, E. Caetano, Vibration based structural health monitoring of an arch bridge: From automated OMA to damage detection, *Mech. Syst. Signal Process.* 28, 212-228, 2012.

[10] H. Hotelling, Multivariate quality control-illustrated by the air testing of sample bombsights, *in: Techniques of Statistical Analysis*, 111-184, 1947.

[11] G. Curioni, *L'arte del costruire: costruzioni civili, stradali ed idrauliche* (in Italian), Augusto Federico Negro Editore, Turin, Italy, 1873.

[12] F. Fassi, C. Achille, Relazione delle attività di rilievo topografico e laser-scanner: Ponte dell'Olla località Gaiola (CN) (in Italian), Technical report, Politecnico di Milano, 2018.

[13] S. Taricco, *Il tramvai di Demonte: ricordi di una storia passata* (in Italian), Mauro Fantino Editore, Borgo San Dalmazzo, Italy, 2001.

[14] B. Peeters. G. De Roeck, Reference-based stochastic subspace identification for output-only modal analysis, *Mech. Syst. Signal Process.* 13(6), 855-878, 1999.

[15] A. Cabboi, F. Magalhães, C. Gentile, A. Cunha, Automated modal identification and tracking: Application to an iron arch bridge, *Struct. Control Health Monit.* 24(1), e1854, 2017.

[16] R. Brincker, L. Zhang, P. Andersen, Modal identification of output-only systems using frequency domain decomposition. *Smart Mater. Struct.* 10(3), 441-445, 2001.

[17] B. M. Douglas, W. H. Reid, Dynamic tests and system identification of bridges, *J. Struct. Div. ASCE* 108(10), 2295-2312, 1982.

[18] J. Kennedy, R. Eberhart, Particle Swarm Optimization, *in: Proceedings of IEEE International Conference on Neural Networks*, 1942-1948, 1995.

[19] I. Venanzi, A. Kita, N. Cavalagli, L. Ierimonti, F. Ubertini, Earthquake-induced damage localization in an historic masonry tower through long-term dynamic monitoring and FE model calibration, *Bull. Earthq. Eng.* 18(5), 2247-2274, 2020.